

Static critical behavior of three-dimensional classical Heisenberg models: A high-resolution Monte Carlo study

Kun Chen, Alan M. Ferrenberg, and D. P. Landau

Center for Simulational Physics, The University of Georgia, Athens, Georgia 30602

(Received 21 January 1993)

Using both recently developed cluster-algorithm and histogram methods, we have carried out a high-resolution Monte Carlo study of static critical properties of classical ferromagnetic Heisenberg models. Extensive Monte Carlo simulations were performed at several temperatures in the critical region, using an improved cluster-updating scheme, on $L \times L \times L$ simple-cubic and body-centered-cubic systems with $L \leq 40$. Thermodynamic quantities as a function of temperature in the vicinity of the critical point were obtained by an optimized multiple-histogram method, and the critical temperature and static critical exponents were extracted using finite-size scaling. Our best estimates for the inverse critical temperatures are 0.693 035(37) for the simple-cubic system and 0.486 798(12) for the body-centered-cubic system. Estimated static critical exponents for both systems agree with each other within their respective error bars, and the mean estimates $\nu=0.7048(30)$ and $\gamma=1.3873(85)$ are also in excellent agreement with field-theoretic predictions 0.705(3) and 1.386(4).

I. INTRODUCTION

Three-dimensional classical ferromagnetic Heisenberg spin systems with simple-cubic (sc), body-centered-cubic (bcc), and face-centered-cubic (fcc) structures are traditional models for the study of critical phenomena.¹⁻⁷ Although a great deal of effort has been devoted over the years to investigating critical behavior in these models through a variety of approaches, discrepancies still exist between results obtained with different methods. Using high-temperature series expansions, Ritchie and Fisher² calculated the inverse critical temperature and static critical exponents for all three systems. Their results for the bcc and fcc systems were confirmed by a later extended recalculation.³ However, their estimate for the inverse critical temperature of the sc system, 0.6916(2), was contradicted by the extended recalculation, which yielded 0.6924(2) and 0.6925(1) based on the Padé approximant and ratio methods, respectively. Nightingale and Blöte⁵ performed a transfer-matrix Monte Carlo study and found the inverse critical temperature for the sc system to be 0.6922(2) and 0.6925(3) from fitting to data with different smallest system sizes, which supported the extended recalculation. They did not have results for the bcc system but their estimates for the fcc system were larger than those from high-temperature series expansions.²⁻⁴ Estimated static critical exponents for the three systems by high-temperature series expansions, transfer-matrix Monte Carlo techniques, and field theory⁶ also differ from each other.

Computer simulations using Monte Carlo methods provide an independent way to study critical phenomena. One must, however, deal with finite systems and use finite-size scaling^{8,9} to predict properties of the infinite system. Consequently, not only must a large number of effectively independent measurements be made in the vicinity of the critical point to ensure good statistics, but the system sizes must also be chosen large enough that

corrections to finite-size scaling are not large compared to the other statistical and systematic errors.¹⁰ It may therefore be very difficult to simultaneously satisfy these requirements within limited computer resources because of the many simulations needed to determine the locations and magnitudes of the extrema of thermodynamic quantities accurately for finite-size scaling and because of critical slowing down. Due to these difficulties, early Monte Carlo simulations were not able to produce accurate results.^{7,11} However, recent developments in simulation techniques and data-analysis methods, together with improvement in computer performance, have made it possible to carry out high-resolution Monte Carlo studies.^{12,13}

The histogram method has provided a highly efficient technique to extract accurate information over the entire scaling region from a small number of simulations.^{12,13} Peczak *et al.*⁷ performed long Monte Carlo simulations for the sc system at temperatures just *above* the critical value and used an optimized multiple-histogram method to analyze their data. They predicted the inverse critical temperature to be 0.6929(1), which is higher than previous estimates, and obtained various static critical exponents which are in agreement with field theoretic predictions.⁶ However, their precision was limited by relatively small system sizes ($6 \leq L \leq 24$) and by critical slowing down in the Metropolis algorithm they used.

Cluster algorithms have proven to be extremely effective in reducing critical slowing down.^{13,14} They are nonlocal updating techniques in which a single cluster or many clusters of spins are constructed and updated simultaneously. Dimitrović *et al.*¹⁵ employed this method to study the sc system of size L up to 96 at temperatures *below* the critical value. With a two-step fitting they obtained the inverse critical temperature to be 0.6930(2). Unfortunately the number of measurements they performed seems too small considering the relatively large systems in their study.

Monte Carlo estimates for the inverse critical temperature of the sc system are consistently larger than results from high-temperature series expansions and transfer-matrix Monte Carlo techniques. Although the inverse critical temperature is not a universal parameter, the accuracy of its value strongly affects the accuracy in current Monte Carlo estimates for static critical exponents. Recently, efforts have been made to use both the cluster algorithm and the histogram method in Monte Carlo studies.^{16–18} In this paper we present results of a high-resolution Monte Carlo study of static critical properties of the sc and bcc classical Heisenberg models; the results are based on a mass of data which was generated over a temperature range covering the critical region for system sizes up to $L = 40$ with an improved cluster-updating scheme and which was then analyzed with an optimized multiple-histogram method. The models, simulation techniques, and data-analysis methods are described in Sec. II. Results and discussions are presented in Sec. III and a summary is given in Sec. IV.

II. BACKGROUND

A. Models

The classical Heisenberg models we are interested in are isotropic ferromagnetic spin systems on either sc or bcc lattices. The Hamiltonian for such systems is given by

$$\mathcal{H} = -J \sum_{\langle ij \rangle} \mathbf{S}_i \cdot \mathbf{S}_j, \quad (1)$$

where J is the ferromagnetic coupling constant and the spin $\mathbf{S}_i = (S_i^x, S_i^y, S_i^z)$ is of $O(3)$ symmetry and unit length in the spin space. We consider $L \times L \times L$ systems with nearest-neighbor interactions and periodic boundary conditions, so that the sum in Eq. (1) runs over all nearest-neighbor pairs of lattice sites. Note that a bcc lattice consists of two identical interpenetrating sc lattices and thus has twice as many spins as does a sc lattice with the same linear dimension.

The basic thermodynamic quantities of interest are the total energy $E = -J \sum_{\langle ij \rangle} \mathbf{S}_i \cdot \mathbf{S}_j$ and the magnetization $m = L^{-3} [(\sum_i S_i^x)^2 + (\sum_i S_i^y)^2 + (\sum_i S_i^z)^2]^{1/2}$. For simplicity we will set the ferromagnetic coupling constant J and the Boltzmann constant equal to 1.

B. Simulation

It has been demonstrated that Wolff's single-cluster algorithm together with his embedding technique are very effective in reducing critical slowing down for $O(n)$ ferromagnetic spin models.^{14,16,19} In the original cluster algorithm proposed by Swendsen and Wang²⁰ for the Potts model, a configuration of activated bonds is constructed from the spin configuration and clusters of spins are formed based on the bond configuration. To update the spin configuration, each cluster is assigned randomly a new spin value and the same value is given to all spins in the same cluster. Rather than building and flipping many clusters of spins, Wolff suggested growing only a single

cluster from a randomly chosen site and flipping the entire cluster of spins. This single-cluster algorithm is very successful when applied to the Ising model.²¹ For spin systems with continuous symmetry, Wolff further developed an embedding technique to introduce Ising variables into $O(n)$ models.¹⁴ One starts by choosing a direction in the spin space at random and breaking up each spin variable into two components with one perpendicular and the other either parallel or antiparallel to the randomly chosen direction. An Ising model is then constructed by assigning $+1$ to spins of parallel components and -1 to spins of antiparallel components. The couplings between nearest-neighbor Ising spins are determined by the products of these parallel and antiparallel components and are therefore random in magnitude but are all ferromagnetic so no frustration or competing interactions are present.²² Such a random-bond Ising model can be efficiently simulated with the single-cluster algorithm and the original $O(n)$ model can be correspondingly updated by changing the sign of parallel or antiparallel components of spins in the same cluster.

We introduce here another scheme based on the same embedding idea^{14,22,23} for the cluster updating of the $O(n)$ model. It consists of four steps:

(i) Choose a randomly oriented n -dimensional orthogonal coordinate system, find all new components of spins in the randomly chosen coordinate system, and generate independent random-bond Ising models for each axis direction;

(ii) For each resultant random-bond Ising model, choose a lattice site randomly and build a single cluster with a bond-activating probability

$$P_{ij}^k = \begin{cases} 1 - \exp(-2KS_i^k S_j^k) & \text{if } S_i^k S_j^k > 0 \\ 0 & \text{otherwise} \end{cases}, \quad (2)$$

where S_i^k is the k th component of \mathbf{S}_i in the new coordinate system and $k = 1, 2, \dots, n$. $K = 1/T$ is the inverse temperature with the coupling constant J and the Boltzmann constant being 1;

(iii) Flip all single clusters of embedded Ising variables and update the $O(n)$ spin configuration;

(iv) Repeat (ii) and (iii) several times before returning to (i).

Detailed balance is satisfied and ergodicity is guaranteed in this multiple embedding, multiple single-cluster-updating scheme. Note that in this scheme, if individual measurements are made after each single-cluster flipping and are combined properly, the total number of measurements can easily be increased by one or two orders of magnitude at a small expense of computer time, even though the number of independent measurements is not increased.²⁴ Applications of the scheme showed that it dramatically reduces critical slowing down and has an improved efficiency over the original Wolff algorithm. Results of further exploration of this improved scheme will be reported in a later publication.

The Heisenberg model is a special case of the general $O(n)$ model for $n = 3$. With the improved cluster-updating scheme we performed multiple Monte Carlo simulations on sc and bcc classical Heisenberg systems

with $20 \leq L \leq 40$ over a temperature range spanning the critical region. All simulations were done using the University of Georgia high-performance, hierarchical facility consisting of an IBM ES/9000 vector supercomputer linked to a cluster of IBM RISC/6000 workstations.

It has been noticed²⁵ in Monte Carlo simulations of the two-dimensional Ising model using cluster algorithms that certain random number generators can lead to systematic errors which greatly exceed the statistical errors, due to subtle correlations in the pseudorandom number sequences. In our simulations, random numbers were produced by a subtract-with-carry generator²⁶ and no systematic deviations were found between results obtained with a hybrid Metropolis and overrelaxation algorithm,²⁷ Wolff's single-cluster algorithm, and our improved cluster-updating scheme, using both this random number generator and others.²⁵ We believe that the embedding technique creates a random-bond Ising model with enough randomness in the bond-activating probabilities to destroy the effects of the correlations which produced errors in the simple Ising model.

All simulations were carried out at temperatures close to the previous best estimates for T_c . For sc systems, simulations were carried out with $L = 20, 24,$ and 32 at three temperatures corresponding to $K = 0.6929, 0.6930,$ and 0.6931 and with $L = 28, 36,$ and 40 at $K = 0.69306$. For bcc systems, simulations were performed with $L = 20, 24, 28,$ and 32 at $K = 0.4870$ and with $L = 36$ and 40 at $K = 0.48685$. Simulations were also carried out for each system at two different temperatures, one above and one below T_c , close to the peak positions of the specific-heat and finite-lattice susceptibility. In each simulation, 1×10^6 measurements were made after enough single-cluster updatings (1×10^4 to 7×10^4) were carried out for equilibration. The interval of measurement was decided by step (iv) of the improved cluster-updating scheme, in which steps (ii) and (iii) were repeated twice in our simulations. At least two simulations were performed with different random number seeds for every system size at each temperature. The total number of measurements obtained for a given temperature was estimated to be at least 5×10^4 times the measured integrated energy autocorrelation time. Values of the total energy and magnetization from each measurement were stored as a data list for histogram analysis.

C. Histogram analysis

The histogram method has been applied with great success to the study of critical phenomena.^{7,12} In a multiple-histogram approach^{28,29} the energy density of states is estimated by combining histograms from simulations performed at several temperatures and minimizing the estimated error in the density of states for each energy value. The energy probability distribution at other temperatures then follows from the optimized estimate for the energy density of states:

$$W(E) = \frac{\sum_i H_i(E)}{\sum_i N_i \exp(-K_i E - f_i)}, \quad (3)$$

as

$$P(E, K) = W(E) \exp(-KE - f), \quad (4)$$

where E is the total energy of the system and f is the reduced free energy at the inverse temperature K , $\exp(f) = \sum_E W(E) \exp(-KE)$. N_i is the total number of entries in the i th histogram $H_i(E)$. The reduced free energy f_i at K_i can be determined self-consistently, up to an additive constant, from the normalization conditions of $P(E, K_i)$:

$$\exp(f_i) = \sum_E \frac{\sum_j H_j(E)}{\sum_j N_j \exp(-K_j E - f_j)} \exp(-K_i E). \quad (5)$$

Knowing the energy probability distribution, one can calculate the thermodynamic average of any function of the energy easily.

To deal with thermodynamic quantities other than the energy, one can choose to work with multidimensional histograms and multidimensional probability distributions. The feasibility of this approach, however, is limited by the available computer memory. A more practical approach is to work with the energy probability distribution and *microcanonical averages* of the quantities of interest.²⁹ In this latter way, the canonical average of a thermodynamic quantity, say Q , can be calculated as a function of inverse temperature K :

$$\langle Q \rangle = \frac{\sum_E Q(E) P(E, K)}{\sum_E P(E, K)}, \quad (6)$$

where $Q(E)$ denotes the microcanonical average obtained directly from simulations:

$$Q(E) = \frac{\sum_t Q_t \delta_{E_t, E}}{\sum_t \delta_{E_t, E}}. \quad (7)$$

We used the optimized multiple-histogram method to determine the temperature dependence of a number of thermodynamic quantities according to Eqs. (6) and (7).

Because the energy spectrum of a Heisenberg spin system is continuous, the data list obtained from a simulation is basically a histogram with one entry per energy value. In order to use the histogram method efficiently, we divided the energy range $E \leq 0$ evenly into 30 000, 100 000, and 300 000 bins and reconstructed histograms. In early testing, results from the three binnings as well as the data list agreed with each other within statistical errors. Therefore, although 30 000 bins would have been sufficient, we chose to use 100 000 bins throughout our studies just to be cautious.

For all system sizes, histograms obtained from simulations overlap sufficiently on both sides of the critical point so that the statistical uncertainty in the wings of the histograms^{7,12} near the critical point may be suppressed by using the optimized multiple-histogram method. Therefore the locations and magnitudes of the extrema of thermodynamic quantities can be determined accurately to extract the critical temperature and static critical exponents from their finite-size scaling behavior.

D. Finite-size scaling

According to the finite-size scaling theory,^{8,9} for a sufficiently large system at a temperature T close enough to the infinite-lattice critical point T_c , the reduced free-energy density can be divided into a singular part f_s plus a nonsingular background f_{ns} :

$$f(t, H; L) = f_s(t, H; L) + f_{ns}(t, L), \quad (8)$$

where $t = (T_c - T)/T_c$ is the reduced temperature and H is the external ordering field. The nonsingular part is assumed size independent under periodic boundary conditions:

$$f_{ns}(t; L) = f_{ns}(t; \infty). \quad (9)$$

The singular part is described phenomenologically by a universal scaling form

$$f_s(t, H; L) = L^{-d} Y(atL^{1/\nu}, bHL^{\Delta/\nu}) + \dots, \quad (10)$$

where a and b are metric factors making the scaling function Y universal, d is the dimension of the system (equal to 3 in our case), and ν and Δ are static critical exponents. Scaling forms for various thermodynamic quantities can be obtained from appropriate derivatives of the free-energy density. Some of them, such as those for the magnetization, susceptibility, and specific heat in zero field, are

$$m \approx L^{-\beta/\nu} \mathcal{M}(tL^{1/\nu}), \quad (11)$$

$$\chi \approx L^{\gamma/\nu} \mathcal{X}(tL^{1/\nu}), \quad (12)$$

$$c \approx c_\infty(t) + L^{\alpha/\nu} \mathcal{C}(tL^{1/\nu}), \quad (13)$$

where α , β , γ , and δ are also static critical exponents and satisfy the scaling and hyperscaling relations³⁰

$$\Delta = \beta\delta = \beta + \gamma, \quad (14)$$

$$2 - \alpha = d\nu = 2\beta + \gamma. \quad (15)$$

Derivatives and logarithmic derivatives of the magnetization are important thermodynamic quantities for studying critical phenomena.¹² We define here some related quantities useful in determining the critical temperature T_c and the critical exponent ν , in our own notations, as follows:

$$V_1 \equiv 4[m^3] - 3[m^4], \quad (16)$$

$$V_2 \equiv 2[m^2] - [m^4], \quad (17)$$

$$V_3 \equiv 3[m^2] - 2[m^3], \quad (18)$$

$$V_4 \equiv (4[m] - [m^4])/3, \quad (19)$$

$$V_5 \equiv (3[m] - [m^3])/2, \quad (20)$$

$$V_6 \equiv 2[m] - [m^2], \quad (21)$$

where

$$[m^n] \equiv \ln \frac{\partial \langle m^n \rangle}{\partial T}. \quad (22)$$

From Eq. (11) it is easy to show that

$$V_j \approx (1/\nu) \ln L + \mathcal{V}_j(tL^{1/\nu}) \quad (23)$$

for $j=1, 2, \dots, 6$. At the critical temperature T_c ($t=0$) the \mathcal{V}_j should be constants independent of the system size L .

Information about the critical exponent ν and the critical temperature T_c is also contained in the scaling behavior of the extrema of thermodynamical quantities. According to Eqs. (11) and (12), locations of the extrema of the following quantities

$$\chi = L^3 \langle (m - \langle m \rangle)^2 \rangle / T, \quad (24)$$

$$D_{K_2} \equiv \frac{\partial \langle (m - \langle m \rangle)^2 \rangle}{\partial T}, \quad (25)$$

$$D_{K_3} \equiv \frac{\partial \langle (m - \langle m \rangle)^3 \rangle}{\partial T}, \quad (26)$$

$$D_{K_4} \equiv \frac{\partial \langle (m - \langle m \rangle)^4 \rangle - 3 \langle (m - \langle m \rangle)^2 \rangle^2}{\partial T}, \quad (27)$$

$$U_3 \equiv \frac{\langle (m - \langle m \rangle)^3 \rangle}{\langle m \rangle \langle (m - \langle m \rangle)^2 \rangle}, \quad (28)$$

$$U_4 \equiv \frac{3 \langle (m - \langle m \rangle)^2 \rangle^2 - \langle (m - \langle m \rangle)^4 \rangle}{3 \langle m^2 \rangle^2}, \quad (29)$$

vary asymptotically as

$$T_c(L) \approx T_c + a_q L^{-1/\nu}, \quad (30)$$

where a_q is a quantity-dependent constant.

Equations (11)–(13), (23), and (30), together with the scaling and hyperscaling relations, provide effective ways to estimate the critical temperature and static critical exponents. It should be noted, however, that these equations are valid only in the asymptotic regime. If L is not large enough or T is too far from T_c , corrections to scaling and/or finite-size scaling may be needed due to irrelevant scaling fields or nonlinearities in the scaling variables.^{31,32}

III. RESULTS

A. Determinations of ν and T_c

By using the analysis discussed in the previous section, we can simultaneously estimate both ν and T_c by scanning over the critical region and looking for a quantity-independent slope. Figure 1 gives an example of such an effort and Fig. 2 presents scanning results for the sc system. In Fig. 1 the estimated error bars for individual points are smaller than the sizes of the points. The error bar shown in Fig. 2 is twice the averaged error estimate for slopes from linear fits to points in Fig. 1. From both figures we estimate that $1/\nu = 1.4212(46)$ and $K_c = 0.69304(4)$. Correspondingly, we have $\nu = 0.7036(23)$ and $T_c = 1.44292(8)$ for the sc system. In the same way we obtain $\nu = 0.7059(37)$ and $T_c = 2.0542(2)$ for the bcc system. It is worth pointing out that the estimated values of ν for both systems agree

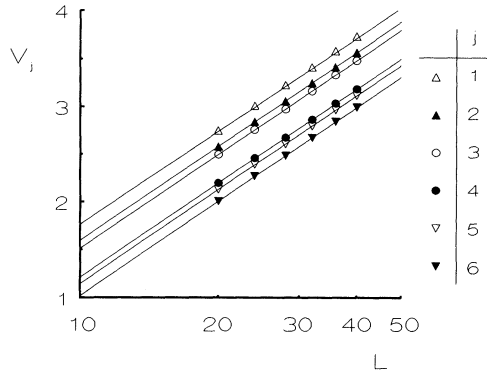


FIG. 1. Size dependence of V_j at $K=0.69304$ with $j=1, 2, \dots, 6$ for the sc system. Straight lines are linear fits to the data and have the same slope (1.4212).

with each other within their error bars, indicating, as expected,³³ that the two systems belong to the same universality class.

Another way to estimate ν and T_c is to look into the scaling behavior of the locations $T_c(L)$ of the extrema in thermodynamic quantities. Because of the limited number of different system sizes, rather than performing a nonlinear fit with Eq. (30) to get ν and T_c , we use the previously estimated value for ν to extract T_c from $T_c(L)$ by a linear fit, as shown in Fig. 3 for the sc system. In the figure the estimated error bars for individual points are smaller than the sizes of the points. Note that Eq. (29) defines a reduced fourth-order cumulant which is different from the simple Binder parameter⁷ and has a minimum very close to T_c . From the average of the intercepts we obtain $T_c=1.442929(77)$ or $K_c=0.693035(37)$. These values agree very well with previous estimates from Figs. 1 and 2. With the new estimate for T_c the critical exponent ν is recalculated in the same way as illustrated in Fig. 1 and we find that $1/\nu=1.4216(46)$, or $\nu=0.7034(23)$. Results for ν and T_c obtained in the two different approaches are self-

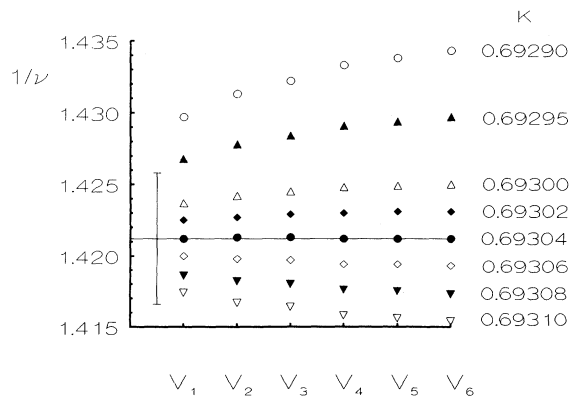


FIG. 2. Quantity dependence of scanning results for the sc system as explained in the text. The horizontal line is drawn at $1/\nu=1.4212$.

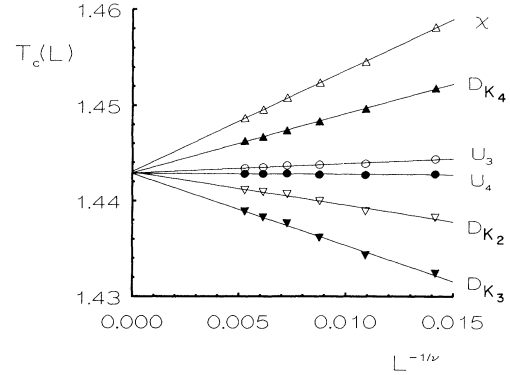


FIG. 3. Size dependence of the locations of the extrema in different thermodynamic quantities with $\nu=0.7036$ for the sc system.

consistent. For the bcc system we obtain $T_c=2.054241(52)$ or $K_c=0.486798(12)$ from Fig. 4.

In using Eqs. (23) and (30) to determine ν and T_c we have assumed that the asymptotic regime is reached and the corrections to finite-size scaling can be neglected. This assumption is supported in part by early results^{7,18} that indicated, within the errors of the data, the asymptotic finite-size scaling regime was already reached by $L=10$ or $L=12$. In Fig. 5 a scaling plot is drawn in accordance with Eq. (30) for the sc system. Because there are no systematic errors visible in the figure, this approximation seems reasonable, at least within our resolution limit.

It has been shown¹² that the magnitudes of the extrema of some thermodynamic quantities, such as the derivative of the simple Binder parameter and logarithmic derivatives of $\langle m^n \rangle$, can also be used to determine the critical exponent ν without any consideration of T_c . Unfortunately we find that locations of these extrema are quite far from T_c so that corrections to scaling for these quantities are presumably quite significant. The value of ν estimated in this way is consistent with our previous esti-

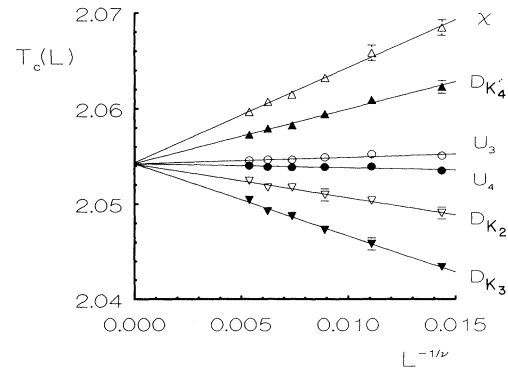


FIG. 4. Size dependence of the locations of the extrema in different thermodynamic quantities with $\nu=0.7059$ for the bcc system. When not shown, the estimated error bars are smaller than the symbols.

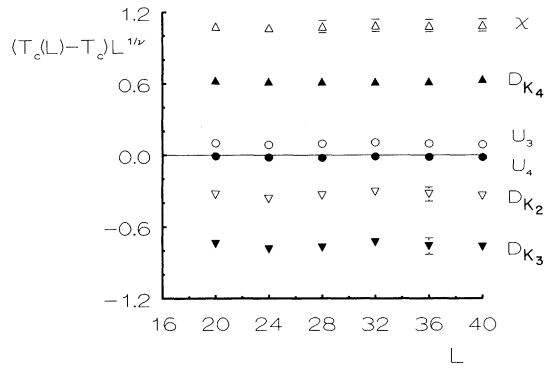


FIG. 5. Scaling behavior of the locations of the extrema in different thermodynamic quantities with $T_c = 1.442\,929$ and $\nu = 0.7036$ for the sc system.

mates but has a much larger error bar.

Combining results obtained using two different approaches, we find our best estimates for the critical exponent ν and the critical point are $\nu = 0.7036(23)$ and $K_c = 0.693\,035(37)$ for the sc system and $\nu = 0.7059(37)$ and $K_c = 0.486\,798(12)$ for the bcc system.

B. Determinations of other critical exponents

With ν and T_c determined accurately we can now extract the critical exponent γ from the scaling properties of the susceptibility in two ways. From Eq. (12) it is clear that the peak value of the finite-lattice susceptibility given by Eq. (24) and the magnitude of the true susceptibility at T_c (given by the same equation with $\langle m \rangle = 0$) are both proportional to $L^{\gamma/\nu}$ asymptotically. Plotted in Fig. 6 are their scaling behaviors and linear fits for the sc system. Estimated error bars for individual points are again smaller than the sizes of the points. The slope of the bottom straight line is $1.9775(20)$ from the linear fit. The slope for the top one is $1.9725(50)$, where the error bar includes the uncertainty in the slope resulting from the uncertainty in our estimate for T_c .⁷ Within their respective error bars, the slopes of the two straight lines

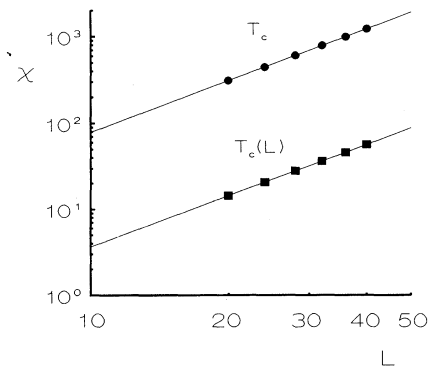


FIG. 6. Log-log plot of size dependence of the finite-lattice susceptibility at $T_c(L)$ and the true susceptibility at $T_c = 1.442\,929$ for the sc system.

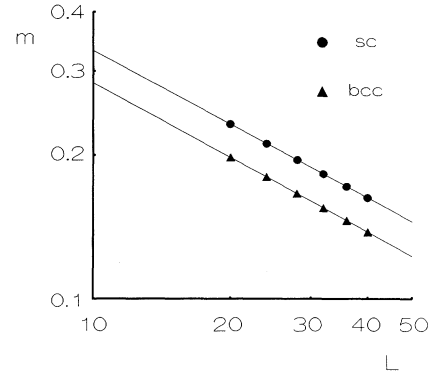


FIG. 7. Log-log plot of size dependences of the magnetization for the sc system at $T_c = 1.442\,929$ and for the bcc system at $T_c = 2.054\,241$.

are in agreement, as expected, thus supporting our estimates for ν and T_c . The ratio of exponents γ/ν obtained from the average of the slopes is $1.9750(35)$; therefore, $\gamma = 1.3896(70)$ for the sc system. For the bcc system we obtain $\gamma = 1.385(10)$.

All the other critical exponents can be calculated by using the estimates for ν and γ and the scaling and hyperscaling relations, such as Eqs. (14) and (15). For example, we find that β and α are $0.3606(24)$ and $-0.1108(69)$ for the sc system and $0.3664(54)$ and $-0.118(11)$ for the bcc system.

According to Eq. (11), at the critical point, the magnetization varies asymptotically as $L^{-\beta/\nu}$. Figure 7 is a log-log plot of size dependence of the magnetization at T_c for both systems. From the figure we can estimate β/ν directly. We then have $\beta = 0.3616(31)$ for the sc system and $0.3669(32)$ for the bcc system. Again the error bars include the influence of the uncertainty in our estimate for T_c . These direct results confirm the previous values calculated by scaling and hyperscaling relations.

In our simulations we have measured the specific heat c from the fluctuations of the total energy as $c = (\langle E^2 \rangle - \langle E \rangle^2) / (T^2 L^3)$. In principle, the critical ex-

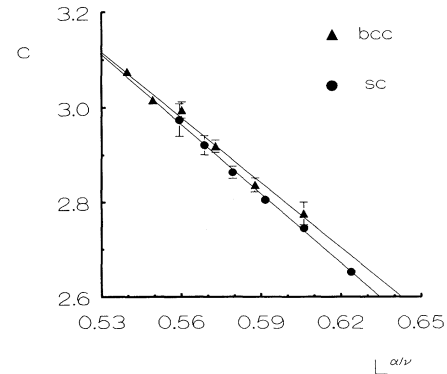


FIG. 8. Size dependences of the specific heat for the sc system with $\alpha/\nu = -0.158$ at $T_c = 1.442\,929$ and for the bcc system with $\alpha/\nu = -0.167$ at $T_c = 2.054\,241$.

TABLE I. A comparison of results with different methods for the sc classical Heisenberg model. The superscript indicates that values are calculated using scaling and hyperscaling relations [Eqs. (14) and (15)].

	Series expansions			Transfer-matrix Monte Carlo	Monte Carlo			This study
	Ref. 2	Ref. 3	Ref. 34	Ref. 5	Ref. 7	Ref. 15	Ref. 18	
K_c	0.6916(2)	0.6925(1)	0.6929(1)	0.6925(3)	0.6929(1)	0.6930(2)	0.6930(1)	0.693 035(37)
ν	0.705(10)		0.712(10)	0.716(40)	0.706(9)	0.73(4)	0.704(6)	0.7036(23)
γ	1.375(15)	1.395(5)	1.40(1)		1.390(23)			1.3896(70)
β					0.364(7)	0.36(2)	0.362(4)	0.3616(31)
β^{cal}								0.3606(24)
α^{cal}					-0.118(18)		-0.112(18)	-0.1108(69)

ponent α can then be determined from the scaling behavior of the specific heat at T_c by a nonlinear least-squares fit using Eq. (13) with $t=0$. However, because of our limited number of data points, results from three-parameter nonlinear fits are not well defined. Rather than performing the nonlinear fit we chose to accept the previously calculated α value and use a linear fit to determine the other two parameters $c_\infty(0)$ and $\mathcal{C}(0)$. This is done in Fig. 8 and we estimate that $c_\infty(0)$, the specific heat for the infinite lattice at T_c , is 5.70(12) and $\mathcal{C}(0)$ is -4.89(11)k for the sc system. For the bcc system we get 5.54(14) and -4.58(25), respectively. The negative values of α and $\mathcal{C}(0)$ indicate that, around T_c , the behavior of the specific heat is cusplike rather than divergent for both systems.

C. Discussion

Our results for the sc system are given in Table I. Also listed in the table are some existing Monte Carlo results, including the one obtained recently by Holm and Janke¹⁸ using Wolff's single-cluster algorithm, as well as estimates obtained from other methods. As one can see from the table, our estimate for the inverse critical temperature is consistent but slightly larger than existing Monte Carlo results. The estimated error bar, however, is smaller. On the other hand, our estimate for K_c is certainly larger than results obtained from other methods such as high-temperature series expansions [K_c ranging from 0.6916(2)

to 0.6925(1)]^{2,3} and transfer-matrix Monte Carlo [$K_c=0.6922(2), 0.6925(3)$].⁵ Within the error bars, our combined estimates for ν and K_c agree with other listed Monte Carlo and recent series expansion results³⁴ but reduce the range of uncertainty significantly. In Fig. 9 we present a comparison of high-resolution estimates for ν and K_c from different methods. The boxes represent the quoted error bars in both ν and K_c assuming independent errors. Also plotted in the figure is the prediction for ν by field theory⁶ which does not give an estimate for K_c .

Results for the bcc system are presented in Table II. Our estimates for the inverse critical temperature and critical exponents are consistent with the result from extended high-temperature series expansions,³ but have smaller error bars. So far we have not found any other high-quality Monte Carlo data about this system in the literature.

Within their respective error bars, our estimates for the critical exponents for both systems agree with each other and are consistent with early Monte Carlo results for the fcc system³⁵ which have large errors. Table III lists field theoretic predictions⁶ for those critical exponents, which are independent of lattice structures, as well as results of high-temperature series expansions averaged over the sc, bcc, and fcc systems.² Our estimates also agree with these theoretical predictions and suggest that the "best estimates" from series analysis are slightly too low. Included in the table are our final estimates for the critical exponents, which are obtained by averaging results for both sc and bcc systems. The agreement between our final estimates and the field theoretic predictions is excel-

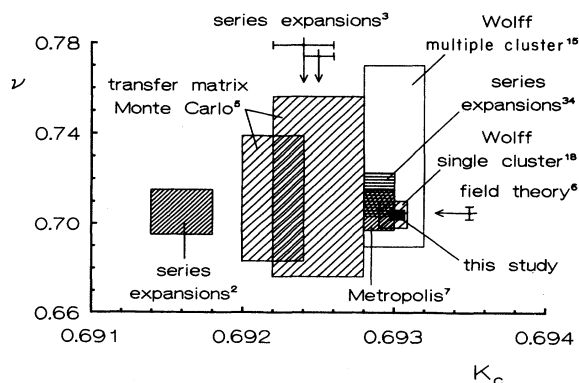


FIG. 9. A comparison of high-resolution estimates for ν and K_c from different methods for the sc system.

TABLE II. A comparison of results obtained with different methods for the bcc classical Heisenberg model. The superscript indicates that values are calculated using scaling and hyperscaling relations [Eqs. (14) and (15)].

	Series expansions		Monte Carlo
	Ref. 2	Ref. 3	This study
K_c	0.486 35(10)	0.4868(4)	0.486 798(12)
ν	0.700(5)		0.7059(37)
γ	1.38(1)	1.393(5)	1.385(10)
β			0.3669(32)
β^{cal}			0.3664(54)
α^{cal}			-0.118(11)

TABLE III. Theoretical predictions and our final estimates for static critical exponents of the three-dimensional classical Heisenberg model.

	Series expansions Ref. 2	Field theory Ref. 6	Monte Carlo This study
ν	$0.7025^{+0.010}_{-0.005}$	0.705 ± 0.0030	0.7048 ± 0.0030
γ	$1.375^{+0.02}_{-0.01}$	1.386 ± 0.0040	1.3873 ± 0.0085
β		0.3645 ± 0.0025	0.3639 ± 0.0035
α		-0.115 ± 0.009	-0.1144 ± 0.0090

lent and provides convincing numerical evidence for the conjecture³³ that both systems, and perhaps the fcc system, belong to the same universality class.

IV. CONCLUSIONS

The static critical properties of classical ferromagnetic Heisenberg models have been studied using large-scale Monte Carlo computer simulations. We have obtained precision equivalent to (or better) than that found with

any other method. In order to achieve this degree of precision we have employed a multiple-embedding, multiple single-cluster algorithm to reduce critical slowing down in updating spin configurations. Extensive Monte Carlo simulations performed over a temperature range covering the critical region have made it possible to acquire accurate information on critical properties with an optimized multiple-histogram method. Using the finite-size scaling theory we estimate that the inverse critical temperature is 0.693 035(37) for the simple-cubic system and 0.486 798(12) for the body-centered-cubic system. Our estimates for the static critical exponents for both systems agree with each other and with field theoretic predictions. This result substantiates the conjecture that both systems belong to the same universality class; our final estimates for static critical exponents, which are mean results of those for the two systems, are $\nu=0.7048(30)$ and $\gamma=1.3873(85)$.

ACKNOWLEDGMENT

This research was supported in part by National Science Foundation Grant No. DMR-9100692.

- ¹C. Domb and M. F. Sykes, Phys. Rev. **128**, 168 (1962).
²D. S. Ritchie and M. E. Fisher, Phys. Rev. B **5**, 2668 (1972).
³S. McKenzie, C. Domb, and D. L. Hunter, J. Phys. A **15**, 3899 (1982).
⁴M. Ferrer and A. Hamid-Aidinejad, Phys. Rev. B **34**, 6481 (1986).
⁵M. P. Nightingale and H. W. J. Blöte, Phys. Rev. Lett. **60**, 1562 (1988).
⁶J. C. LeGuillou and J. Zinn-Justin, J. Phys. (Paris) Lett. **46**, L137 (1985); Phys. Rev. B **21**, 3976 (1980) and references therein.
⁷P. Peczak, A. M. Ferrenberg, and D. P. Landau, Phys. Rev. B **43**, 6087 (1991) and references therein.
⁸M. N. Barber, in *Phase Transitions and Critical Phenomena*, edited by C. Domb and J. L. Lebowitz (Academic, New York, 1983), Vol. 8, p. 145.
⁹*Finite Size Scaling and Numerical Simulation of Statistical Systems*, edited by V. Privman (World Scientific, Singapore, 1990).
¹⁰A. M. Ferrenberg, D. P. Landau, and K. Binder, J. Stat. Phys. **63**, 867 (1991).
¹¹M. Jochims, T. Holey, and M. Föhnle, Phys. Status Solidi B **166**, 277 (1991).
¹²A. M. Ferrenberg and D. P. Landau, Phys. Rev. B **44**, 5081 (1991) and references therein.
¹³For a review see R. H. Swendsen, J.-S. Wang, and A. M. Ferrenberg, in *The Monte Carlo Method in Condensed Matter Physics*, edited by K. Binder (Springer-Verlag, Heidelberg, 1992), p. 75.
¹⁴U. Wolff, Phys. Rev. Lett. **62**, 361 (1989); Nucl. Phys. B **322**, 759 (1989).
¹⁵I. Dimitrović, P. Hasenfratz, J. Nager, and F. Niedermayer, Nucl. Phys. B **350**, 893 (1991).
¹⁶W. Janke, Phys. Lett. A **148**, 306 (1990).
¹⁷K. Chen, A. M. Ferrenberg, and D. P. Landau, J. Appl. Phys. **73**, 5488 (1993).
¹⁸C. Holm and W. Janke, Phys. Lett. A **173**, 8 (1993).
¹⁹R. G. Edwards and A. D. Sokal, Phys. Rev. D **40**, 1374 (1989).
²⁰R. H. Swendsen and J.-S. Wang, Phys. Rev. Lett. **58**, 86 (1987).
²¹P. Tamayo, R. C. Brower, and W. Klein, J. Stat. Phys. **58**, 1083 (1990).
²²D. Kandel and E. Domany, Phys. Rev. B **43**, 8539 (1991).
²³R. C. Brower, N. A. Gross, and K. J. M. Moriarty, J. Comput. Phys. **95**, 167 (1991).
²⁴It has recently been observed that errors from histogram reweighting depend not only on the number of *independent* measurements made, but also on the *total* number. A. M. Ferrenberg, D. P. Landau, and R. H. Swendsen (unpublished).
²⁵A. M. Ferrenberg, D. P. Landau, and Y. J. Wong, Phys. Rev. Lett. **69**, 3382 (1992).
²⁶G. Marsaglia, B. Narasimhan, and A. Zaman, Comput. Phys. Commun. **60**, 345 (1990).
²⁷K. Chen and D. P. Landau, Phys. Rev. B **46**, 937 (1992).
²⁸A. M. Ferrenberg and R. H. Swendsen, Phys. Rev. Lett. **63**, 1195 (1989).
²⁹A. M. Ferrenberg, in *Computer Simulation Studies in Condensed Matter Physics III*, edited by D. P. Landau, K. K. Mon, and H.-B. Schüttler (Springer-Verlag, Heidelberg, 1991).
³⁰V. Privman, P. C. Hohenberg, and A. Aharony, in *Phase Transitions and Critical Phenomena*, edited by C. Domb and J. L. Lebowitz (Academic, New York, 1991), Vol. 14, p. 1.
³¹F. J. Wegner, Phys. Rev. B **5**, 4529 (1972).
³²A. Aharony and M. E. Fisher, Phys. Rev. B **27**, 4394 (1983).
³³L. P. Kadanoff, in *Critical Phenomena, Proceedings of the E. Fermi International School of Physics*, edited by M. S. Green (Academic, New York, 1971), Vol. 51, p. 100.
³⁴J. Adler, C. Holm, and W. Janke (private communication).
³⁵Th. T. A. Paauw, A. Compagner, and D. Bedeaux, Physica A **79**, 1 (1975).